energies

MDPI

Article

A Frequency Control Strategy Considering Large Scale Wind Power Cluster Integration Based on Distributed Model Predictive Control

Bohao Sun [1,*], Yong Tang [1], Lin Ye [2], Chaoyu Chen [2], Cihang Zhang [2] and Wuzhi Zhong [1]

[1] China Electric Power Research Institute, Haidian District, Beijing 100192, China; tangyong@epri.sgcc.com.cn (Y.T.); zhongwz@epri.sgcc.com.cn (W.Z.)

[2] College of Information and Electrical Engineering, China Agricultural University, Beijing 100083, China; yelin@cau.edu.cn (L.Y.); chenchaoyu@cau.edu.cn (C.C.); zhangch@cau.edu.cn (C.Z.)

* Correspondence: hobson_choice@126.com; Tel.: +86-010-8281-2508

Received: 7 May 2018; Accepted: 12 June 2018; Published: 19 June 2018

Abstract: With large scale wind integration and increasing wind penetration in power systems, relying solely on conventional generators for frequency control is not enough to satisfy system frequency stability requirements. It is imperative that wind power have certain capabilities to participate in frequency control by cooperating with conventional power sources. Firstly, a multi-area interconnected power system frequency response model containing wind power clusters and conventional generators is established with consideration of several nonlinear constraints. Moreover, a distributed model predictive control (DMPC) strategy considering Laguerre functions is proposed, which implements online rolling optimization by using ultra-short-term wind power forecasting data in order to realize advanced frequency control. Finally, a decomposition-coordination control algorithm considering Nash equilibrium is presented, which realizes online fast optimization of multivariable systems with constraints. Simulation results demonstrate the feasibility and effectiveness of the proposed control strategy and algorithm.

Keywords: wind power cluster; distributed model predictive control (DMPC); frequency control; Nash equilibrium decomposition-coordination

1. Introduction

As a significant and mature renewable energy generation technology, wind power has been extensively applied in China, and nowadays there are many large scale wind power systems integrated into the power supply. However, wind has inherent intermittence and volatility, which result in uncertain power output characteristics. Moreover, wind power almost makes no contribution to system frequency control due to the converter, which rapidly increases the frequency control pressure on conventional generators. In order to guarantee secure and stable operation of power systems, it is urgent to research how wind power clusters could actively participate in system frequency control [1–6].

Currently, both domestic and foreign studies can mainly be classified into three categories according to their spatial level: wind turbine, wind farm and wind power cluster [7]. At the wind turbine level, frequency control research is relatively mature enough, mainly including rotor inertia control [8–10], rotor over-speed control [11,12], pitch control [13,14] and composite control [15,16]. At the wind farm and wind power cluster level, there are many studies on hierarchical control frameworks for active power dispatch [17,18]. Nevertheless, from the power system point of view, only a few studies have focused on system frequency control strategies with coordination of wind power clusters and conventional generators.

In recent years, the control theory adopted in industrial process named model predictive control (MPC), which consists of prediction model, rolling optimization and feedback correction, has been widely applied in wind power control research. This control theory uses prediction models to calculate the dynamic process of a prediction horizon under a definite control effect. Afterwards, according to the constraints and optimal objectives, rolling optimization solves the optimization problem and implements the present control sequence. Meanwhile, feedback correction updates the prediction model according to the real measurement information at each time-step [19–23].

In the active power dispatch aspect, Ye et al. [24] divided wind turbines into groups according to the generation status, and rolling optimization is utilized at the wind farm level, wind turbines level and single turbine level, which implements multi-objectives coordination optimization control. Makarov et al. [25] proposed a method to estimate the uncertainty of balancing capacity, ramping capability, and ramp duration requirements with forecasting data, and a new technique was proposed to evaluate the forecasting generation performance envelope for the worst-case scenario. Zhang et al. [26] used MPC and large system hierarchical control theory to establish a hierarchical MPC mechanism, and it was applied to active power dispatch scenarios containing large scale wind power integration. Kaddah et al. [27] proposed a nonlinear MPC integrated with a swarm optimization technique to describe the nonlinear behavior in the mathematical formulation, which is called swarm model predictive control (SMPC) optimization, and it considers both unit commitment and economic dispatch problems incorporating wind power. Xie and Ilic [28,29] applied MPC to solve multi-objective economic/environmental dispatch problems in power systems with intermittent resources and construct a forecasting optimal algorithm to dispatch the available generation resources aiming to minimize both generation and environmental costs.

In the frequency control aspect, Variani and Tomsovic [30] illustrated that the existing automatic generation control (AGC) can be substituted by a two-tier structure of local control operating with flatness-based control, which can decompose the multiple machine system into multiple nonlinear controllable systems in a canonical form, and this makes it easier to design and implement compared with conventional AGC. Mohamed et al. [31] adopted centralized MPC to complete area frequency control with the consideration of interconnected system. Mohamed et al. [32] made use of decentralized MPC to realize dimensionality reduction, which is beneficial to online rolling optimization. However, there are no information sharing and coordinated mechanism among each sub-controller. In [33,34], the merit of dimensionality reduction is retained and on account of this, there exist information communication and coordination of every controller when objective optimization is carried on in local controller, which constitutes a form of distributed MPC (DMPC) and improves performance and stability in system frequency control with wind power participation. Venkat et al. [35] presented a DMPC framework that is suitable for controlling large-scale power systems, and AGC is simulated to demonstrate the proposed framework. Furthermore, a new intelligent agent-based control scheme with Bayesian networks is presented to design AGC system in a multi-area power system [36], and the multi-agent structure in the proposed control framework has been proved to have a high degree of scalability. In [37,38], a multi-area interconnected power system with wind turbines integration based on DMPC for frequency control was proposed, and a frequency response model of three-area power system concerning the aggregated wind turbine model is introduced. Casavola [39] presented a distributed sequential reference-offset governor scheme which could solve load frequency supervision and coordination problems with constraints in multi-area microgrids.

Nevertheless, the studies mentioned above still have three problems: (1) during the process of wind power actively participating in frequency control, many studies do not make the most of ultra-short-term wind power forecasting information; (2) the conventional frequency control is attached to the ACE control method belonging to lag correction control from the point view of temporal scale, which goes against system security and stability; (3) centralized MPC is not suitable for online optimization control, as decentralized MPC cannot guarantee the global optimality of computation due to the lack of communication among controllers, and it is not fully considered in DMPC how to

adjust certain decomposition and coordination algorithm in order to coordinate wind power clusters and conventional generators in the aspect of system frequency control.

Therefore, an advanced frequency control strategy with consideration of large scale wind power clusters integration in multi-area interconnected power system based on DMPC is proposed in this paper. Firstly, the strategy establishes a multi-area interconnected power system frequency response model including wind power clusters and conventional generators, which considers wind power ramp rate, dead zone of conventional generators and other nonlinear constraints. Moreover, a DMPC strategy with the consideration of ultra-short-term wind power forecasting data is presented, which implements rolling optimization to realize advanced frequency control and stabilize power fluctuation of tie-lines. In order to realize parameter dimensionality reduction, Laguerre function is used in this section. Finally, a Nash equilibrium decomposition-coordination online optimization algorithm is proposed to solve DMPC optimization problems containing Laguerre functions. The simulation results indicate that the proposed strategy can effectively implement coordination among wind power clusters and conventional generators in frequency control. Also, the algorithm satisfies speed requirement of multi-variable online rolling optimization, which proves the effectiveness and robustness of the proposed control strategy.

2. Proposed Model

The multi-area interconnected power system consists of several control areas, and every two areas are connected by an area tie-line. In each area, a disturbance caused by a load change or other events may initiate a frequency transient variation of the entire power system, which needs automation generation control (AGC) units accept generation control signals from controllers to maintain the frequency stability. In China, the function of AGC is mostly undertaken by conventional thermal units. However, in some control areas containing wind power clusters, the installed wind power capacity is relatively large compared with the thermal power capacity. Moreover, wind power exhibits inherent characteristics of randomness, intermittence and fluctuation. Therefore, under this situation, it is not reliable for the safe and stable operation of the system just relying on the conventional power frequency control methods when load disturbances occur. In this section, a multi-area interconnected system frequency response model containing large scale wind power clusters and conventional generators considering nonlinear constraints is proposed.

2.1. The State Space Equations

It is assumed that interconnected power system has N control areas, and the block diagram of control area i is shown in Figure 1. Parameters and variables are summarized in Table 1. By applying the "virtual inertia control method" described in [40–42], doubly-fed induction generator wind turbines can provide effective inertia support to reduce the system frequency change rate in the initial period with disturbances, and therefore corresponding "inertia time constant of wind farms" is provided. The state space equations have considered many nonlinear constraints, such as dead zone limits of conventional generators $\sigma_i(\cdot)$, generation rate of conventional generators and generation rate of wind farms. At each initial moment of the calculation time-steps, a local DMPC controller will accept ACE signals and execute the necessary online computations using its internal control strategy and algorithm, which can obtain an optimal control sequence for this time-step. Also, the optimal control sequence is applied to the conventional generators section and wind power clusters section, which forms ΔP_{ti} and ΔP_{WF} to dynamically compensate the load variation $\Delta P_{\mathrm{L}i}$ and tie-line power variation $\Delta P_{\mathrm{tie},i}$ at this time-step, respectively. Consequently, the purpose of wind power clusters coordinating with conventional generators to undertake frequency control can be achieved.

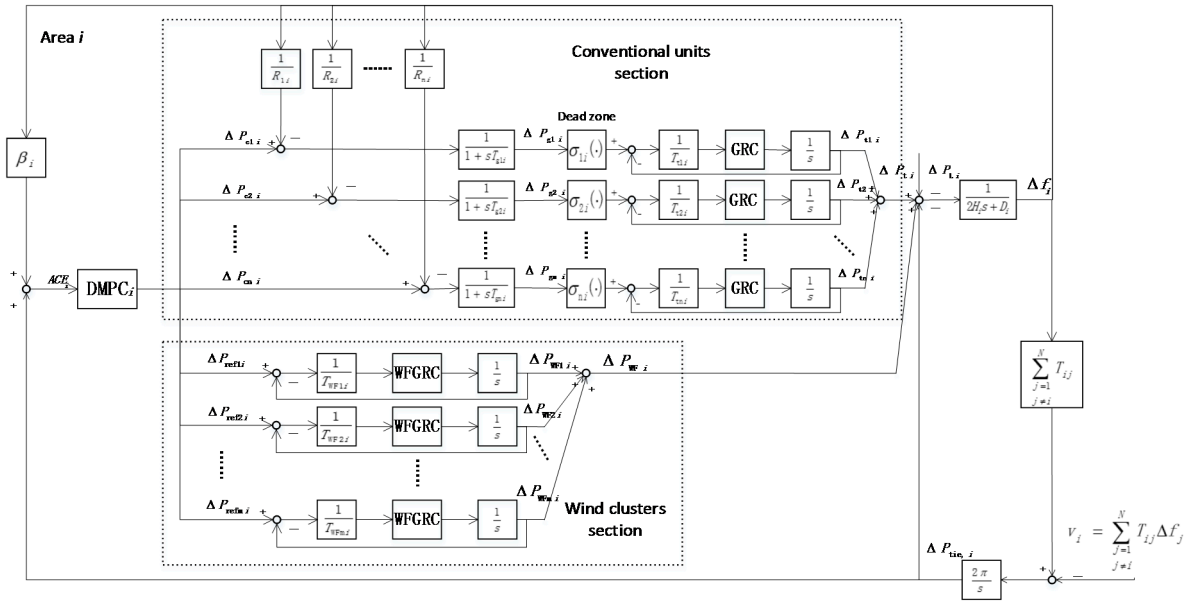

Figure 1. Frequency response model of multi-area interconnected power system.

Table 1. Parameters and variables.

Parameter	Meaning	Unit
N	Number of interconnected areas	-
n	Number of conventional generators	-
m	Number of wind farms	-
$\sigma_{1i}(\cdot), \sigma_{2i}(\cdot), \ldots, \sigma_{ni}(\cdot)$	Dead zone of generator governor	-
GRC	Generation rate of generators	-
WFGRC	Generation rate of wind farms	-
β_i	Frequency deviation factor	pu/Hz
$R_{1i}, R_{2i}, \ldots, R_{ni}$	Droop characteristics of generators	Hz/pu
$T_{g1i}, T_{g2i}, \ldots, T_{gni}$	Time constant of generator governor	s
$T_{t1i}, T_{t2i}, \ldots, T_{tni}$	Time constant of generator steam turbine	s
$T_{WF1i}, T_{WF2i}, \ldots, T_{WFmi}$	Inertia time constant of wind farms	s
H_i	Equivalent inertia coefficient of system	s
D_i	Equivalent damping coefficient of system	pu/Hz
T_{ij}	Synchronous coefficient of tie-line	pu
V_i	Area interface quantity	pu·Hz
State variable	**Meaning**	**Unit**
$\Delta P_{g1i}, \Delta P_{g2i}, \ldots, \Delta P_{gni}$	Position change of generator governor	pu
$\Delta P_{t1i}, \Delta P_{t2i}, \ldots, \Delta P_{tni}$	Power change of generators	pu
$\Delta P_{WF1i}, \Delta P_{WF2i}, \ldots, \Delta P_{WFmi}$	Power change of wind farms	pu
Δf_i	Area frequency variation	Hz
$\Delta P_{tie,i}$	Power change of tie-line	pu
Control variable	**Meaning**	**Unit**
$\Delta P_{c1i}, \Delta P_{c2i}, \ldots, \Delta P_{cni}$	Control order for conventional generators from DMPC controller	pu
$\Delta P_{ref1i}, \Delta P_{ref2i}, \ldots, \Delta P_{refmi}$	Control order for wind power clusters from DMPC controller	pu
Output variable and disturbance variable	**Meaning**	**Unit**
ACE_i	Area control error	pu
ΔP_{Li}	Area load variation	pu

According to Figure 1 and Laplace transformation, the state space equations can be obtained:

$$\Delta \dot{f}_i = \frac{1}{2H_i}(\Delta P_{ti} + \Delta P_{WFi} - \Delta P_{tie,i} - \Delta P_{Li} - D_i \Delta f_i) \quad (1)$$

where $\Delta P_{ti} = \Delta P_{t1i} + \Delta P_{t2i} + \cdots + \Delta P_{tni}$, $\Delta P_{WFi} = \Delta P_{WF1i} + \Delta P_{WF2i} + \cdots + \Delta P_{WFmi}$.

$$\Delta\dot{P}_{\text{tie},i} = 2\pi\left(\sum_{j=1,j\neq i}^{N} T_{ij}\Delta f_i - \sum_{j=1,j\neq i}^{N} T_{ij}\Delta f_j\right) \tag{2}$$

$$\Delta\dot{P}_{\text{g1}i} = \frac{1}{T_{\text{g1}i}}\left(\Delta P_{\text{c1}i} - \frac{1}{R_{1i}}\Delta f_i - \Delta P_{\text{g1}i}\right) \tag{3}$$

$$\Delta\dot{P}_{\text{t1}i} = \frac{\sigma_{1i}(\cdot)}{T_{\text{t1}i}}\Delta P_{\text{g1}i} - \frac{1}{T_{\text{t1}i}}\Delta P_{\text{t1}i} \tag{4}$$

$$\Delta\dot{P}_{\text{WF1}i} = \frac{1}{T_{\text{WF1}i}}\left(\Delta P_{\text{ref1}i} - \Delta P_{\text{WF1}i}\right) \tag{5}$$

In this paper, ACE is selected as the area output variable, since it can represent not only area frequency deviations, but also the tie-line power fluctuations. The output equation is shown as:

$$y = \beta_i\Delta f_i + \Delta P_{\text{tie},i} \tag{6}$$

2.2. Deposition of Nonlinear Constraints

2.2.1. Deposition of Dead Zone of Conventional Generator Governors

Referring to [43], the T-S fuzzy model method is used to deal with the nonlinear dead zone constraints of conventional generator governors. If a control area has n conventional generators, the corresponding state equations have 2^n possibilities. The merits of this approach are that it only needs to consider the worst equation of 2^n possible state equations and can convert nonlinear dead zone constraints into linear parameters, which is convenient for subsequent discrete computation.

2.2.2. Deposition of Conventional Generators and Wind Farms Generation Rate Constraints

The nonlinear generation rate constraints of conventional generators and wind farms can be managed in two ways. Firstly, adding state variables constraints for $\Delta P_{\text{t1}i}$, $\Delta P_{\text{t2}i}$, ... , $\Delta P_{\text{tn}i}$ and $\Delta P_{\text{WF1}i}$, $\Delta P_{\text{WF2}i}$, ... , $\Delta P_{\text{WFm}i}$ during the process of computing optimal sequence, and thereby solved through being converted into quadratic programming (QP) problem with constraints. Secondly, according to inherent properties of MPC optimization function, modulating weight suppression parameters of internal control variables in MPC optimization function can also achieve the performance of restraining generation rate.

2.3. The Matrix Expression of State Space Equations

Combining the state equations and output equation, and the multi-dimensional continuous state space matrix expression can be obtained as:

$$\begin{cases} \Delta\dot{x}_i = A_{ii\text{c}}\Delta x_i + B_{ii\text{c}}\Delta u_i + F_{ii\text{c}}\Delta d_i + \sum\limits_{i\neq j} A_{ij\text{c}}\Delta x_j \\ y_i = C_{ii\text{c}}\Delta x_i \end{cases} \tag{7}$$

where Δx_i is $(m + 2n + 2)$ dimensional state vector, $\Delta x_i = [\Delta f_i \vdots \Delta P_{\text{tie},i} \vdots \Delta P_{\text{g1}i} \ \ldots \ \Delta P_{\text{gn}i} \vdots \Delta P_{\text{t1}i} \ \ldots \ \Delta P_{\text{tn}i} \vdots \Delta P_{\text{WF1}i} \ \ldots \ \Delta P_{\text{WFm}i}]^{\text{T}}$. Δu_i denotes $(m + n)$ dimensional control vectors, $\Delta u_i = [\Delta P_{\text{c1}i} \ \ldots \ \Delta P_{\text{cn}i} \vdots \Delta P_{\text{ref1}i} \ \ldots \ \Delta P_{\text{refm}i}]^{\text{T}}$. Δd_i is one dimensional disturbance variable, $\Delta d_i = \Delta P_{\text{L}i}$. y_i is one dimensional output variable, $y_i = ACE_i$. $A_{ii\text{c}}$ is $(m + 2n + 2) \times (m + 2n + 2)$ dimensional system matrix. The (2,1) element of $A_{ij\text{c}}$ is $-2\pi T_{ij}$ and other elements are 0. $B_{ii\text{c}}$ is $(m + 2n + 2) \times (m + n)$ dimensional control matrix. $F_{ii\text{c}}$ is $(m + 2n + 2) \times 1$ dimensional disturbance matrix. $C_{ii\text{c}}$ is $1 \times (m + 2n + 2)$ dimensional output matrix.

3. Proposed Control Strategy

3.1. DMPC Considering Laguerre Functions

3.1.1. Determination of Time-Step Duration

In this paper, when discretizing state space model with time-step t_d, t_d should be longer than $T_{g1i} + T_{t1i} + 2H_i + DMPC_i$ and $T_{WF1i} + 2H_i + DMPC_i$, where $DMPC_i$ is the time spent by the DMPC controller for online rolling optimization, and in this way advanced frequency control performance can be achieved at the current time-step. After the system frequency falls, a conventional generator needs about 10–15 s to complete a stable power increase [3] and the system equivalent inertia time constant is about 20 s [44]. Also, it is known that $T_{g1i} + T_{t1i}$ is longer than T_{WF1i}. Therefore, the time-step in this paper is determined as 1 min. Meanwhile, it can be concluded that the shorter computation time spent on online rolling optimization by the DMPC controller, the better frequency advanced control performance could be achieved.

3.1.2. DMPC Considering Laguerre Functions

In order to decrease the heavy computational burden of DMPC, Laguerre functions, which can greatly reduce the number of system parameters and dimensions, are incorporated into DMPC controller to approximate the control trajectory ΔU within the prediction horizon. By merging Equation (7) for all N control areas and discretizing with t_d = 1 min, the global discrete state space equation can be obtained:

$$\begin{cases} \Delta x_m(k+1) = A_d \Delta x_m(k) + B_d \Delta u(k) + F_d \Delta d(k) \\ y(k) = C_d \Delta x_m(k) \end{cases} \tag{8}$$

where A_d, B_d, F_d and C_d denote corresponding discrete-time form of the system matrices in Equation (7).

In order to take into account both $\Delta x_m(k)$ and $y(k)$, and to facilitate DMPC controller design, a new state variable vector $x(k)$ is defined as:

$$x(k) = \begin{bmatrix} \Delta x_m(k) & y(k) \end{bmatrix}^T \tag{9}$$

Discrete augmented state space equations are formatted as:

$$\begin{cases} x(k+1) = Ax(k) + B\Delta u(k) + F\Delta d(k) \\ y(k) = Cx(k) \end{cases} \tag{10}$$

where $\Delta x_m(k)$ is an n_1 dimensional column vector and $n_1 = (m + 2n + 2) \times N$; $\Delta u(k)$ is an n_2 dimensional column vector and $n_2 = (m + n) \times N$; $y(k + 1)$ is an N dimensional column vector.

Define prediction horizon and control horizon as N_P and N_C, respectively. Output vector Y and control input vector ΔU are established with time-step t_d:

$$\begin{cases} Y = \begin{bmatrix} y(k+1|k) & \cdots & y(k+N_P|k) \end{bmatrix}^T \\ \Delta U = \begin{bmatrix} \Delta u(k) & \cdots & \Delta u(k+N_C-1) \end{bmatrix}^T \end{cases} \tag{11}$$

where Y is an N_P dimensional column vector; ΔU is an $N_C \times n_2$ dimensional matrix which is to be calculated by DMPC online rolling optimization, and only the first element is implemented.

Any element in the ΔU matrix is represented by Laguerre function:

$$\Delta u_s(k+s') = L_s(s')^T \eta_s, s = 1, 2, \cdots, n_2, s' = 0, 1, \cdots, N_C - 1 \tag{12}$$

where $L_s(s')^T$ is a standard orthogonal Laguerre sequence and $L_s(s')^T = [l_1^s(s')\ l_2^s(s')\ \dots\ l_\gamma^s(s')]$; η_s is a Laguerre coefficient and $\eta_s = [c_1^s\ c_2^s\ \dots\ c_\gamma^s]^T$. The number of Laguerre function in each control variable is a constant γ instead of control horizon N_C, which is actually only a quarter of N_C. Hence, the number of system parameters can be reduced by about 75% with the consideration of Laguerre functions and the computational burden is greatly reduced.

3.1.3. Prediction Model of DMPC

Divide the B matrix in Equation (10) into $B = [B_1\ B_2\ \dots\ B_{n_2}]$, and the prediction model for output variables at time-step k can be derived by Equation (10):

$$y(k+a|k) = CA^{\alpha}x(k) + C\phi(\alpha)^T\eta + CA^{\alpha-1}F\Delta d(k) \tag{13}$$

where $\alpha = 1, 2, \cdots, N_P$; $\phi(\alpha)^T = \sum_{\beta=0}^{n_2-1} A^{\alpha-\beta-1}[B_1L_2(\beta)^T\ \dots\ B_{n_2}L_{n_2}(\beta)^T]$ and $\eta^T = [\eta_1^T\ \eta_2^T\ \dots\ \eta_{n_2}^T]$.

3.1.4. Rolling Optimization of DMPC

The optimization objective is a combination of output variables tending to 0 in prediction horizon N_P and control variables weight suppression in control horizon N_C starting from time-step k:

$$\min_{\eta} J = \sum_{\alpha=1}^{N_P} \left[y(k+\alpha|k)^T Q y(k+\alpha|k) \right] + \eta^T R_L \eta \tag{14}$$

where Q and R_L are error weight diagonal matrix composed of weight coefficients and control weight diagonal matrix of Laguerre functions, respectively.

Substituting Equation (13) into above equation and expanding:

$$\min_{\eta} J = \eta^T \Omega \eta + 2\eta^T \Phi \tag{15}$$

where η is the optimal control Laguerre coefficient sequence to be solved; $\Omega = \sum_{\alpha=1}^{N_P} \phi(\alpha)C^T Q C \phi(\alpha)^T + R_L$ is a symmetric positive definite matrix; $\Phi = [\sum_{\alpha=1}^{N_P} \phi(\alpha)C^T Q C A^{\alpha}]x(k) + [\sum_{\alpha=1}^{N_P} \phi(\alpha)C^T Q C A^{\alpha-1}F]\Delta d(k)$ can be solved at initial time of each time-step; $x(k)$ and $\Delta d(k)$ could change as time-step rolling in simulation horizon.

Constraints are divided into fixed parts and variable parts, and the fixed parts constraints include three aspects:

(1) State variables constraints:

$$\begin{cases} -\Delta P_{tri,\min} \le \Delta P_{tri} \le \Delta P_{tri,\max} \\ -\Delta P_{WFRi,\min} \le \Delta P_{WFRi} \le \Delta P_{WFRi,\max} \end{cases} \tag{16}$$

where $r = 1, 2, \dots, n$, $R = 1, 2, \dots, m$, $i = 1, 2, \dots, N$. $\Delta P_{tri,\min}$ and $\Delta P_{tri,\max}$ are negative and positive direction generation rate limits of conventional generator; $\Delta P_{WFRi,\min}$ and $\Delta P_{WFRi,\max}$ are negative and positive direction generation rate limits of wind farm.

(2) Control variables constraints:

$$\begin{cases} -\Delta P_{cri,\min} \le \Delta P_{cri} \le \Delta P_{cri,\max} \\ -\Delta P_{refRi,\min} \le \Delta P_{refRi} \le \Delta P_{refRi,\max} \end{cases} \tag{17}$$

where $\Delta P_{cri,\min}$ and $\Delta P_{cri,\max}$ are negative and positive direction DMPC control rate limits of conventional generator; $\Delta P_{refRi,\min}$ and $\Delta P_{refRi,\max}$ are negative and positive direction DMPC control rate limits of wind farm.

(3) Control amplitudes constraints:

$$\begin{cases} -P_{cri,\min} \le P_{cri} \le P_{cri,\max} \\ -P_{refRi,\min} \le P_{refRi} \le P_{refRi,\max} \end{cases} \tag{18}$$

where $P_{cri,\min}$ and $P_{cri,\max}$ are negative and positive direction capacity limits of conventional generator; $P_{refRi,\min}$ and $R_{refRi,\max}$ are negative and positive direction capacity limits of wind farm.

The variable parts impose additional constraints on ΔP_{refRi} considering ultra-short-term wind power forecasting data and current time-step status, which could change at each time-step according to specific conditions. The details of certain judgment process are described in Section 3.2.2.

Adding the variable parts constraints to Equation (18) and combining Equations (16)–(18) by using Laguerre functions:

$$\begin{cases} M_1\eta \le \Delta U_{\max} \\ -M_1\eta \le \Delta U_{\min} \\ M_2\eta \le U_{\max} - u(k-1) \\ -M_2\eta \le U_{\min} + u(k-1) \end{cases} \tag{19}$$

Combining the constraints Equation (19) with the optimization function Equation (15) to obtain a QP problem. Once obtaining the optimal sequence η, the optimal control $\Delta u(k)$ of current time-step k can be calculated under rolling optimization mechanism:

$$\Delta u(k) = \begin{bmatrix} L_1(0)^T & O_2^T & \cdots & O_{n_2}^T \\ O_1^T & L_2(0)^T & \cdots & O_{n_2}^T \\ \vdots & \vdots & \ddots & \vdots \\ O_1^T & O_2^T & \cdots & L_{n_2}(0)^T \end{bmatrix} \eta \tag{20}$$

3.1.5. Feedback Correction of DMPC

At the end of current time-step, the optimal control $\Delta u(k)$ is implemented in the system and the DMPC controller uses the feedback of the state detection equipment to correct Equation (10). In this way, the system discrete state space model equation at next time-step $k+1$ is derived according to actual operating state of the N-area interconnected system. Subsequently, this feedback-corrected system discrete state space model equation in the next time-step $k+1$ is utilized to execute corresponding rolling optimization. This global area state feedback correction is performed every 1 min and loops until the simulation horizon is traversed.

3.2. Method of Wind Power Clusters Actively Participating in Frequency Control

3.2.1. Ultra-Short-Term Wind Power Combination Forecasting Algorithm

In this paper, ultra-short-term wind power forecast is the foundation of wind power clusters participating in frequency control and provides the input data for this research. Three individual prediction methods, which are optimization based on regression power curve (ORPC), least squares support vector machine (LSSVM) and online sequence extreme learning machine (OS-ELM) model are combined to acquire wind power prediction sequence during simulation horizon with a resolution of 15 min. On this basis, the time-varying weight coefficients method [45] is utilized to allocate weight coefficients to three individual prediction methods every 4 h to realize combined forecasting performance:

$$P_{preRi} = \lambda_{1Ri}P_{ORPCRi} + \lambda_{2Ri}P_{LSSVMRi} + \lambda_{3Ri}P_{OS-ELMRi} \tag{21}$$

where P_{preRi} is ultra-short-term forecast wind power of Rth wind farm in ith area; P_{ORPCRi}, $P_{LSSVMRi}$ and $P_{OS-ELMRi}$ are corresponding ORPC, LSSVM and OS-ELM model forecasting power, respectively; λ_{1Ri}, λ_{2Ri} and λ_{3Ri} are model weight coefficients and $\lambda_{1Ri} + \lambda_{2Ri} + \lambda_{3Ri} = 1$.

3.2.2. Judgment Process of Variable Part Constraints

Autoregressive integrated moving average model (ARIMA) is utilized to generate a wind farm power forecasting sequence with a resolution of 1 min under 15 min time window:

$$\begin{bmatrix} P_{k,Ri} & P_{k+1,Ri} & \cdots & P_{k+15,Ri} \end{bmatrix} \tag{22}$$

where k is the current time-step; i is the number of area; $R = 1, 2, \ldots, m$; $P_{k,Ri}$ is wind farm active power real value at current time-step.

Adding predicted power values of m wind farms in the same area at same time-step, the wind power cluster forecasting sequence with a resolution of 1 min in ith area is obtained:

$$\begin{bmatrix} P_{k,i} & P_{k+1,i} & \cdots & P_{k+15,i} \end{bmatrix} \tag{23}$$

Subtracting the first element from the second element in the wind farm power forecasting sequence Equation (22) calculates the wind farm active power trend $\Delta P_{k+1,Ri}$ for the next 1 min at the current time-step. Subtracting the second element from the first element in the area wind power cluster forecasting sequence Equation (23) we obtain area wind power cluster active power trend $\Delta P_{k+1,i}$ for the next 1 min at current time-step:

$$\begin{cases} \Delta P_{k+1,Ri} = P_{k+1,Ri} - P_{k,Ri} \\ \Delta P_{k+1,i} = \sum\limits_{R=1}^{m} P_{k+1,Ri} = \sum\limits_{R=1}^{m} \Delta P_{k+1,Ri} - \sum\limits_{R=1}^{m} \Delta P_{k,Ri} \end{cases} \tag{24}$$

In this paper, the principle of wind power participating in frequency control is defined as follows: at the wind farm level, if $\Delta P_{k+1,Ri} > 0$, the Rth wind farm can be operated in $[0, \Delta P_{k+1,Ri}]$ range through control measures such as pitch angle control (PAC) to provide a certain frequency control capability; if $\Delta P_{k+1,Ri} < 0$, the Rth wind farm loses its frequency regulation ability and its output can only be $\Delta P_{k+1,Ri}$. At the wind power cluster level, if $\Delta P_{k+1,i} > 0$ (or < 0), there may be some wind farms $\Delta P_{k+1,Ri} < 0$ (or > 0) due to spatial distribution, so that $\Delta P_{k+1,i\max}$ and $\Delta P_{k+1,i\min}$ are defined: for terms of $\Delta P_{k+1,Ri} > 0$, sum to acquire $\Delta P_{k+1,i\max}$, make them to 0 and sum to acquire $\Delta P_{k+1,i\min}$. By judging the relationship among $\Delta P_{k+1,i\max}$, $\Delta P_{k+1,i\min}$ and $\Delta P_{Li} + \Delta P_{tie,i}$ calculated at current time-step, the corresponding additional constraints of ΔP_{refRi} are determined as below:

(1) If $\Delta P_{k+1,i\max} < \Delta P_{Li} + \Delta P_{tie,i}$, the additional constraint is $\Delta P_{refRi} = \Delta P_{k+1,Ri}$. At this time, wind power cluster works in maximum power point tracking (MPPT) mode and tries to reduce frequency control burden on conventional generators as much as possible.

(2) If $\Delta P_{k+1,i\min} \leq \Delta P_{Li} + \Delta P_{tie,i} \leq \Delta P_{k+1,i\max}$, for terms with $\Delta P_{k+1,Ri} > 0$, the constraint is $0 < \Delta P_{refRi} < \Delta P_{k+1,Ri}$; for terms with $\Delta P_{k+1,Ri} < 0$, the constraint is $\Delta P_{refRi} = \Delta P_{k+1,Ri}$. At this time, the wind power cluster works in tracking reference power mode and conventional generators can save costs without frequency control action in this time-step.

(3) If $\Delta P_{k+1,i\min} > \Delta P_{Li} + \Delta P_{tie,i}$, for terms with $\Delta P_{k+1,Ri} > 0$, the constraint is $\Delta P_{refRi} = 0$; for terms with $\Delta P_{k+1,Ri} < 0$, the constraint is $\Delta P_{refRi} = \Delta P_{k+1,Ri}$. At this time, wind power cluster works in minimum power mode to prevent over-regulation.

At the end of time-step k, DMPC controller obtains real measured value of $P_{k+1,i}$ through feedback correction. The value is used to replace the second element in Equation (23) to perform feedback

correction to area wind power cluster forecasting model. Then subtracting third element by second element in Equation (23) to obtain the area wind power cluster output trend $\Delta P_{k+2,i}$ for next 1 min at time-step $k+1$. After that, we compare it with $\Delta P_{L,i} + \Delta P_{tie,i}$ at time-step $k+1$, re-enter the above judgment process and perform rolling optimization. Looping operation until the simulation horizon is traversed, and the overall DMPC control strategy is described in Figure 2.

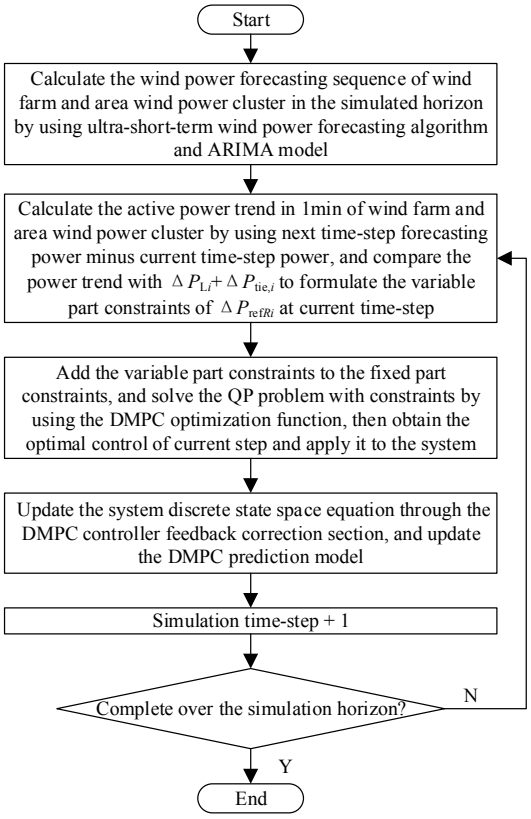

Figure 2. Procedure diagram of DMPC control strategy.

4. Proposed Control Algorithm

Although adding Laguerre functions to the design of the DMPC controller could reduce the number of parameters, it is still a high-dimension concentration online optimization problem considering global variables. The optimization problem not only has multi-variable superposition at the spatial level, but also superposition of control time at the temporal level, so that the burden of online optimization is relatively heavy. In order to reduce the online computational burden, the global optimization function is decomposed into N-areas. The problem of multi-output variables with multi-control variables is transformed into N sub-problems of single output variable and multi-control variables. Each DMPC controller in each area optimizes the predictive control sub-problem to make its own decision, and a coupling optimization process is formed since those sub-problems are related to each other. Therefore, a decomposition-coordination control algorithm based on the concept of Nash optimization in game theory is proposed to make each DMPC controller in each area coordinate with connected ones through communication system. Through the process of finding Nash equilibrium point, each DMPC controller achieves its local optimum, and the optimal control sequence of global area at this time-step is determined.

Transform the optimization function Equation (15) to:

$$\min_{\eta} J = \sum_{i=1}^{N} J_i = \sum_{i=1}^{N} \left(\eta_i^T \Omega_i \eta_i + 2\eta_i^T \Phi_i \right) \tag{25}$$

where η_i is optimal control Laguerre function coefficient in ith area.

Discrete the continuous state space model Equation (7) of ith area by t_d:

$$\Delta x_i(k+1) = A_{iid}\Delta x_i(k) + B_{iid}\Delta u_i(k) + F_{iid}\Delta d_i(k) + \sum_{i\neq j} A_{ijd}\Delta x(k) \tag{26}$$

where $\Delta u_i(k)$ is a $(m + n)$ dimensional control column vector. Divide the B_{iid} matrix into $B = \begin{bmatrix} B_1 & B_2 & \cdots & B_{m+n} \end{bmatrix}$, and according to Equation (26), the prediction model for area state variable at time-step k is derived as:

$$\Delta x_j(k+\alpha|k) = A_{iid}^{\alpha}\Delta x_i(k) + \phi_i(\alpha)^T\eta_i + A_{iid}^{\alpha-1}F_{iid}\Delta d_i(k) + C_{iid}\sum_{i\neq j} A_{iid}^{\alpha-1}A_{ijd}\Delta x_j(k) \tag{27}$$

where $\alpha = 1, 2, \ldots, N_P$, $\eta_i^T = [\eta_1^T\ \eta_2^T\ \ldots\ \eta_{m+n}^T]$, $\phi_i(\alpha)^T = \sum_{\beta=0}^{m+n-1} A_{iid}^{\alpha-\beta-1}[B_1L_1(\beta)^T\ \ldots\ B_{m+n}L_{m+n}(\beta)^T]$.

The optimization function for ith area is:

$$\begin{aligned}\min_{\eta_i} J_i = & \sum_{\alpha=1}^{N_P}\left[y_i(k+\alpha|k)^T Q_i y_i(k+\alpha|k)\right] + \eta_i^T R_{Li}\eta_i = \eta_i^T\left(\sum_{\alpha=1}^{N_P}\phi_i(\alpha)C_{iid}^T Q_i C_{iid}\phi_i(\alpha)^T + R_{Li}\right)\eta_i + \\ & 2\eta_i^T\left\{\left(\sum_{\alpha=1}^{N_P}\phi_i(\alpha)C_{iid}^T Q_i C_{iid}A_{iid}^{\alpha}\right)\Delta x_i(k) + \left(\sum_{\alpha=1}^{N_P}\phi_i(\alpha)C_{iid}^T Q_i C_{iid}A_{iid}^{\alpha-1}F_{iid}\right)\Delta d_i(k) + \right. \\ & \left.\left(\sum_{\alpha=1}^{N_P}\phi_i(\alpha)C_{iid}^T Q_i C_{iid}\sum_{i\neq j}A_{iid}^{\alpha-1}A_{ijd}\right)\Delta x_j(k)\right\}\end{aligned} \tag{28}$$

It can be known from Equation (28) that the optimization function in ith area is related to the state variable $\Delta x_j(k)$ in interconnected areas. Hence, it is a coupling optimization problem and requires coordination among DMPC controllers in each area. The following steps are taken to formulate a decomposition-coordination control algorithm considering Nash equilibrium:

Step 1: Assume initial state $\Delta x_i(k)^{(1)}$ is 0 and iteration number $num = 1$;

Step 2: According to Equation (28) and corresponding constraints, optimal control Laguerre function coefficient $\eta_i^{(num)}$ in each area is calculated;

Step 3: According to extract $\eta_i^{(num)}$ and Equation (27), $\Delta x_i(k)^{(num+1)}$ in each area is calculated;

Step 4: Share $\Delta x_i(k)^{(num)}$ data of each area through the communication system, and Equation (28) is used to calculate the optimal control Laguerre coefficient $\eta_i^{(num+1)}$ in each area. $num = num + 1$;

Step 5: Test iterative termination condition $\|\eta_i^{(num+1)} - \eta_i^{(num)}\| \leq \varepsilon$, where $i \in [1, N]$. If the condition is met, the system is in Nash equilibrium mode. Return $\eta_i^{(num+1)}$ and calculate the current time-step optimal control by using Equation (20). If the condition is not met, return to Step 3.

5. Experimental Examples

In this paper, a three-area interconnected power system is adopted, in which area 1 has a wind power cluster consisting of three wind farms with installed capacities of 172 MW, 121 MW and 202 MW, and area 3 has a wind power cluster consisted of two wind farms with installed capacities of 242 MW and 214 MW. An ultra-short-term wind power combination forecasting algorithm and ARIMA model are utilized to generate wind farm prediction power sequence datasets with a resolution of 1 min in the simulation horizon by using the measured wind speed data on 4 March 2016, as shown in Figure 3. The prediction root mean square errors (RMSE) of the combination forecasting algorithm in this paper is lower than that of monomer forecasting algorithm by comparing with actual active power of each wind farm, which are 7.86% of combination forecasting algorithm, 10.33% of LSSVM and 12.78% of BP neural network, respectively.

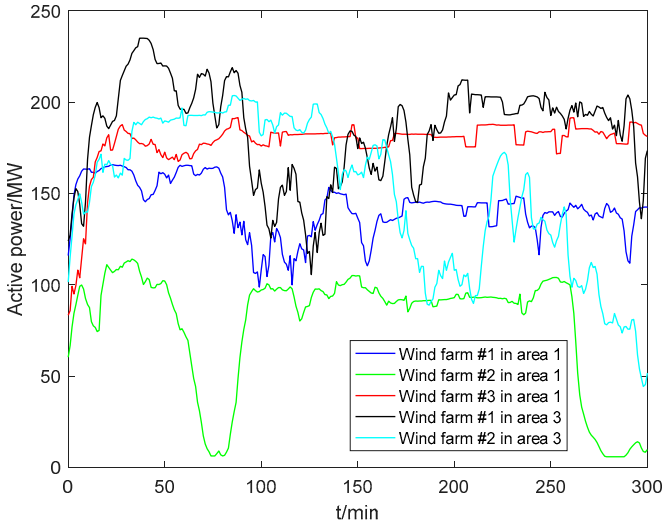

Figure 3. Wind farm prediction power sequence datasets.

Each area has a conventional generator, and each conventional generator capacity and other related parameters are presented in Table 2 with a power base of 1000 MVA. Control horizon, prediction horizon and simulation horizon are set to be 20 min, 50 min and 300 min, respectively. Corresponding Laguerre function pole and function number of each control variable are set to be 0.5 and 10, respectively. In the optimization function, error weight diagonal matrix is set to be N dimensional identity matrix I_N, and control weight diagonal matrix is set to be n_2 dimensional matrix with diagonal element as 0.3. In order to verify the superiority of the proposed control strategy and algorithm, two experimental examples are executed, which consider load step disturbances and load random disturbances, respectively.

Table 2. Parameters of experimental examples.

Parameters	Area 1	Area 2	Area 3
Conventional generators capacity/pu	0.6	0.8	0.6
Generation rate of generators/(pu/min)	0.008	0.008	0.008
β_i/(pu/Hz)	0.3483	0.3473	0.3180
R_i/(Hz/pu)	3	3	3.3
T_{gi}/s	0.8	0.6	0.7
T_{ti}/s	10.0	10.2	9.7
Generation rate of wind farms/(pu/min)	0.006	-	0.006
T_{WFi}/s	2.2/3.3/2.5	-	2.5/3.4
$2H_i$/s	18.0	19.5	18.7
D_i/(pu/Hz)	0.015	0.014	0.015
T_{ij}(pu/Hz)	$T_{12} = 0.20$ $T_{13} = 0.25$	$T_{21} = 0.20$ $T_{23} = 0.12$	$T_{31} = 0.25$ $T_{32} = 0.12$

According to the parameters in Table 2 and multi-area interconnected power system frequency response control block diagram in Figure 1, the Mason formula is utilized to calculate the transfer function of each area and corresponding Bode diagrams are shown in Figure 4. According to the 0 dB line and -180° line in Figure 4, it can be confirmed that the system gain margin and phase margin are 2.4914 dB and 26.0716°, respectively, in area 1, 1.7985 dB and 22.7531°, respectively, in area 2, and 3.2096 dB and 24.7886°, respectively, in area 3. Therefore, the closed loop control system is proven to be stable in the point view of stability margin.

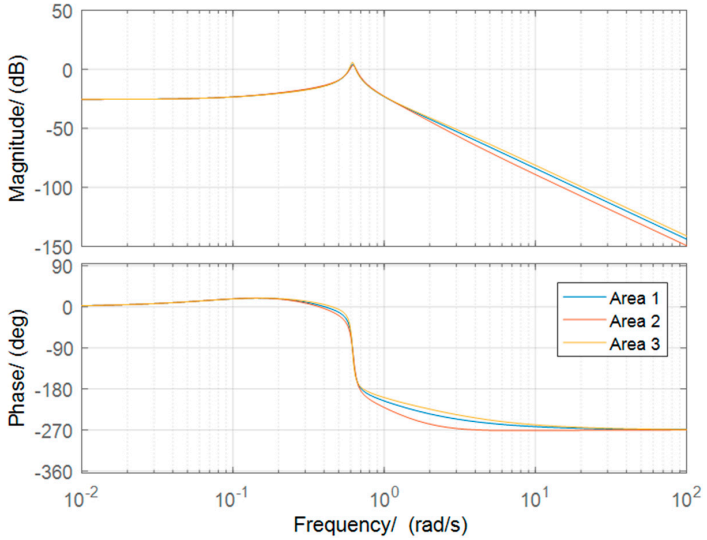

Figure 4. Bode figure of each area control system.

6. Results and Discussion

6.1. Experiment 1: Control Results Considering Load Step Disturbances

In order to clearly reflect the control effects among the methods of proposed DMPC, centralized MPC and decentralized MPC, it is assumed that different load step disturbances occur in three areas. The load step disturbances are set as 50 MW added to area 1 at 50 min, 30 MW added to area 2 at 150 min and 40 MW added to area 3 at 200 min, respectively.

The area frequency deviation curves impacted by load step disturbances in 3-area system are shown in Figure 5, where it can be seen that when the loads suddenly increase, the system frequency decreases due to a power shortage in each area, and the generation supplies need to increase their active power outputs to compensate the shortfall. However, a load step disturbance in one area will result in frequency decreases in the other areas. For instance, when the simulation time is at 50 min, the load of area 1 suddenly increases, and the loads of area 2 and 3 remain unchanged. It can be seen from Figure 5 that frequencies in area 2 and area 3 also decrease, but their decrease amplitudes are smaller than that of area 1. Similar situations also occur when loads of area 2 and 3 suddenly increase. Therefore, certain active power is needed to be extracted in generations of each area at the same time. In Figure 5, from the amplitude comparisons of the area frequency deviations at load step disturbance occurring times, which are 50 min in area 1, 150 min in area 2 and 200 min in area 3, it can be derived that the control performance of centralized MPC is the best. This is because centralized MPC considers global variables and information to perform optimization, and there is no limitation imposing on optimization time in this situation of load step disturbances. It can also be seen that the control performance of proposed MPC is better than that of decentralized MPC, since decentralized MPC method only considers insufficient information of tie-line power in its calculation process. In contrast, the proposed DMPC control strategy has better control accuracy and frequency recovery ability because of its control mechanism of obtaining all information of other areas through high-speed communication system.

Active power control curves of conventional generators and wind farms controlled by proposed DMPC method are shown in Figure 6. It can be observed that wind power clusters controlled by DMPC method can effectively utilize wind energy with consideration of wind power forecasting information and reduce frequency control pressure of conventional generators. When wind power clusters cannot meet frequency regulation requirements alone, conventional generators could be involved in participating in frequency regulation with coordination of related wind power clusters (for example, t = 299 min in area 3).

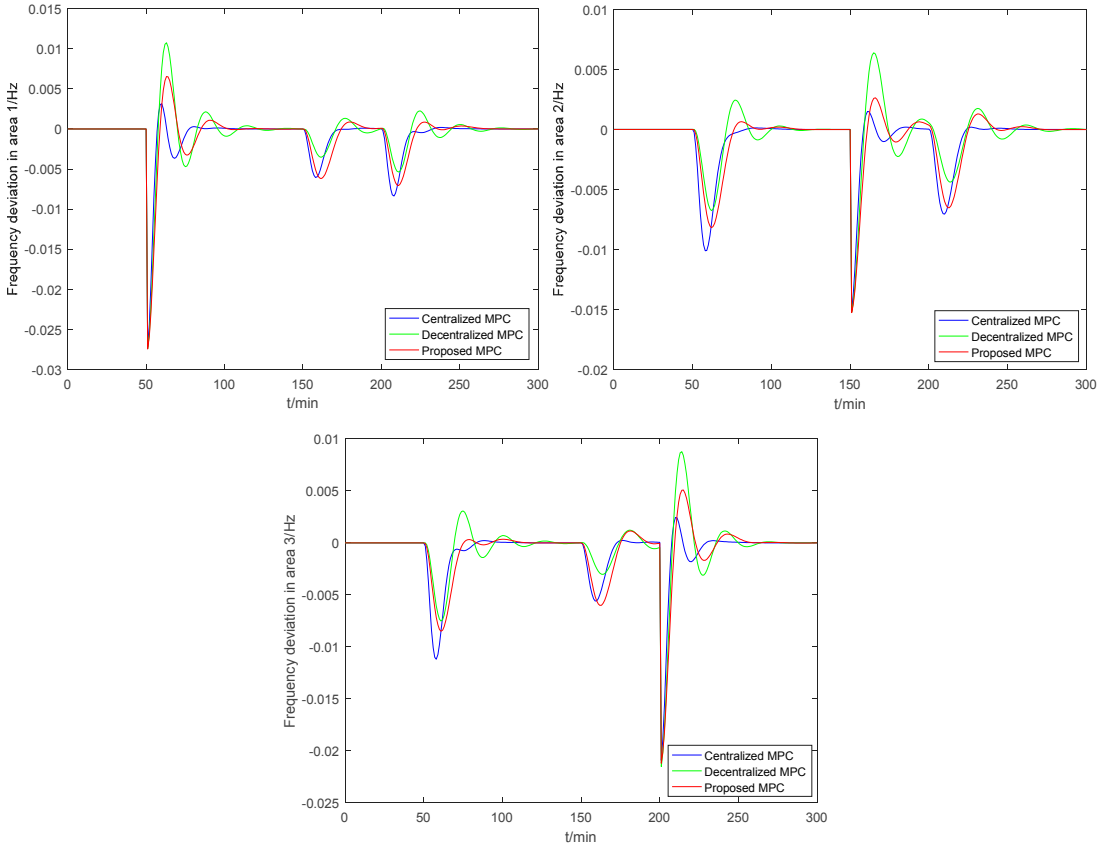

Figure 5. Area frequency deviation curves.

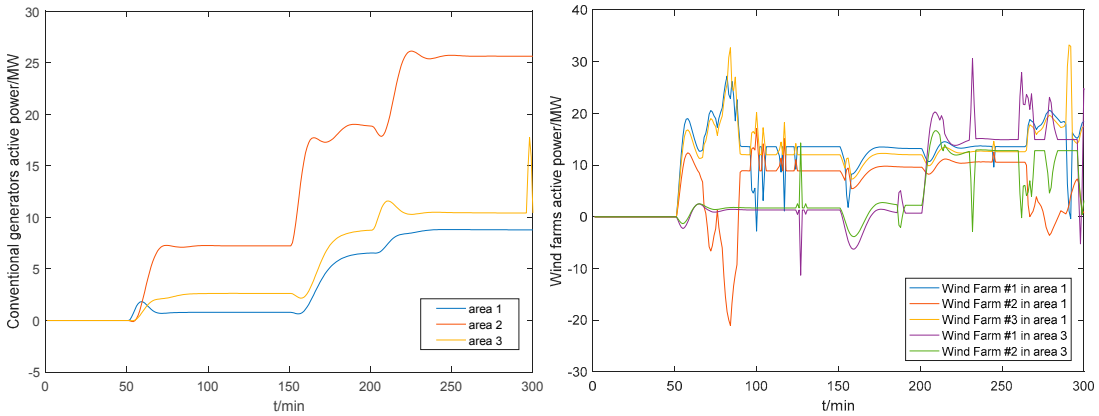

Figure 6. Active power control curves.

6.2. Experiment 2: Control Results Considering Load Random Disturbances

In this experiment, load random disturbances are considered in area 1 and area 3. The load disturbance in each area is divided into two stages in the simulation horizon: the first stage is 1–200 min, in which load disturbance is set to be 1 min resolution evenly distributed random number sequence with amplitude of −30–30 MW in order to consider all variable part constraints stated in Section 3.2.2; the second stage is 201–300 min, in which load disturbance is set to be 0 in order to verify how the disturbance and state variables are stabilized.

The online optimization computational time and frequency adjustment time of each time-step by using decomposition-coordination control algorithm presented in this paper are shown in Table 3, in which a comparison is also made with high-dimensional concentration algorithm considering global

variables. In Table 3, it can be seen that the frequency adjustment time is less than 1 min, so that advanced frequency control could be achieved at each time-step. Table 3 also shows that decomposition-coordination control algorithm saves up to 20.59% computation time than high-dimensional concentration algorithm. It can be further pointed out that decomposition-coordination control algorithm could save more time if the number of conventional generators and wind power clusters increase, since decomposition-coordination control algorithm can be operated in parallel computers to complete computation process and is more suitable for actual engineering application.

Table 3. Computation time and frequency adjustment time comparisons at each time-step.

Algorithm	Computation Time/s	Frequency Adjustment Time/s
Proposed decomposition-coordination control algorithm	2.187	≈42
High-dimensional concentration algorithm	2.754	≈43

In Figure 7, area frequency deviation, tie-line power fluctuation between areas and area ACE deviation curves are shown. It can be observed that in the first stage 1–200 min of load disturbance, the DMPC controller has the ability to control the output of each wind farm appropriately according to wind power forecasting data, so that area wind power cluster could coordinate with conventional generator to participate in frequency control. In this way, the area frequency deviation is controlled in the range of [−0.08, 0.08] Hz, and tie-line power fluctuation between areas and area ACE deviation are controlled in reasonable ranges. It can also be derived that in the second stage 201–300 min of load disturbance, DMPC controller stabilizes the disturbance within 5 time-steps, which makes frequency deviation maintain around zero, and makes tie-line power fluctuation between areas and area ACE deviation maintain around default ratings.

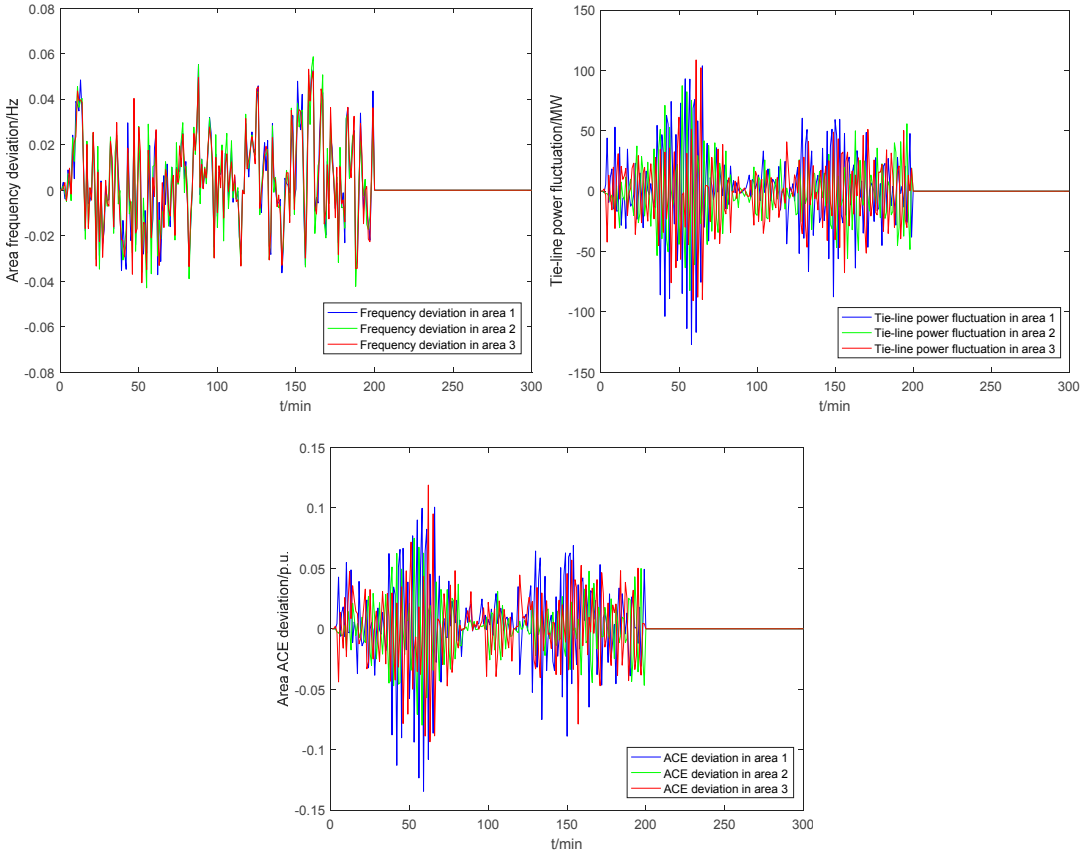

Figure 7. Area main state variables and output variables curves.

In Table 4, the statistics of frequency RMSE in the first stage 1–200 min among DMPC controller, conventional PI controller, centralized MPC controller and decentralized MPC controller are shown, which prove the DMPC controller has more advantages than the other three controllers in frequency control under the condition of wind power fluctuations and load disturbances. Although centralized MPC has the best performance in the situation of step load disturbances stated in Section 6.1, it can be seen in Table 4 that it performs worse in this situation of step random disturbances with a resolution of 1 min. This is because there is not enough time for centralized MPC to accomplish high-dimension concentration online optimization problem considering global variables in just 1 min. In contrast, proposed DMPC divides the control problem of 3-area system into three sub-control problems in the calculation process, and each sub-control problem is calculated by a sub-controller in parallel, which reduces time cost and gets better frequency control performance.

Table 4. Frequency deviation RMSE comparisons in each area.

Control Strategy	Area 1 RMSE/%	Area 2 RMSE/%	Area 3 RMSE/%
Proposed DMPC controller	1.72	1.79	1.71
Conventional PI controller	5.87	6.06	5.76
Centralized MPC controller	5.12	5.19	5.11
Decentralized MPC controller	3.43	3.51	3.40

In Figure 8, optimal control actions of all wind farms at each time-step under DMPC controller are shown. The optimal control is consisted of the first element in optimal control sequence at each time-step, and it is a control pulse signal delivered and applied to each wind farm by DMPC controller. It can be seen that the outputs of all wind farms are controlled in the range of $[-60, 60]$ MW, which is the wind farm output constraint.

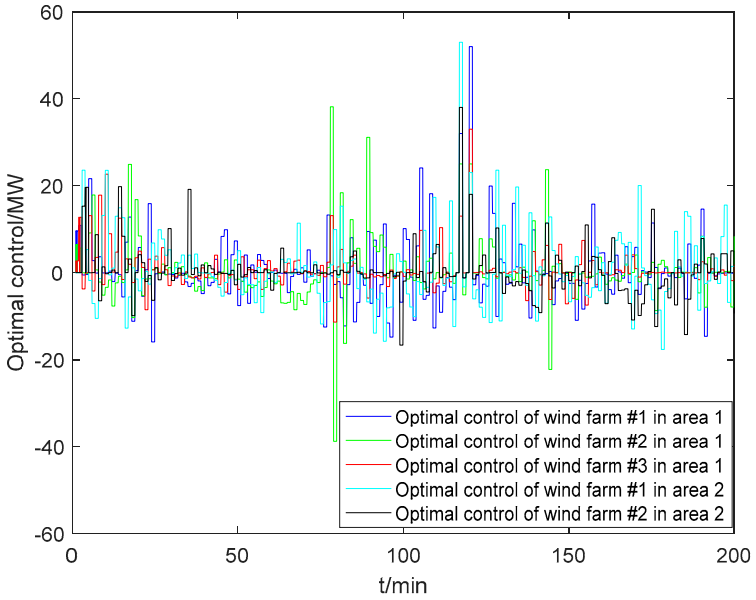

Figure 8. Optimal control applied to each wind farm by DMPC at each time-step.

Table 5 assumes a study scenario where wind power clusters do not participate in frequency control, and only conventional generators undertake all frequency control actions. In Table 5, a comparison is made between wind power clusters participating in frequency control actively by using the control strategy presented in this paper and the study scenario stated above. It can be derived that the mean value of conventional generators absolute control quantities is lower in wind power clusters participating in frequency control actively. Besides, in some time-steps, wind power clusters

have the ability to undertake all frequency control actions under tracking reference power mode, and in this mode conventional generators can save costs without frequency control actions at these certain time-steps, which leads to better economic benefits.

Table 5. Operation cost comparison.

Wind Power Clusters Participate in Frequency Control Actively	The Times That Conventional Generator Do Not Need Control Action	The Mean Value of Conventional Generator Absolute Control Quantities/MW
Conventional generator in area 1	15	7.3
Conventional generator in area 2	15	6.9
Conventional generator in area 3	15	7.2
Wind Power Clusters Do Not Participate in Frequency Control	**The Times That Conventional Generator Do Not Need Control Action**	**The Mean Value of Conventional Generator Absolute Control Quantities/MW**
Conventional generator in area 1	0	8.1
Conventional generator in area 2	0	7.9
Conventional generator in area 3	0	8.2

7. Conclusions

In order to solve the problem that conventional generators cannot guarantee frequency stability alone with large-scale wind power integration, this paper establishes a multi-area interconnected system frequency response model containing conventional generators and wind power clusters. On this basis, a DMPC control strategy considering Laguerre functions is proposed with consideration of ultra-short-term wind power forecasting information, which implements rolling optimization and forms closed-loop control structure via feedback correction. Subsequently, an online decomposition and coordination optimization control algorithm considering Nash equilibrium is proposed to save more computation time. Simulation results indicate that proposed DMPC control strategy can cooperate with conventional generators to actively adjust wind power output considering grids global information and wind power forecasting information, and advanced frequency control at each time-step is achieved. Moreover, tie-line power fluctuation and area ACE deviation are controlled in reasonable ranges. Simulation results also prove that the proposed strategy is cost-effective for conventional generators because of active utilization of wind power resources, which is beneficial to friendly integration of large scale wind power clusters.

Author Contributions: B.S. designed the research and wrote the paper; Y.T. and L.Y. provided professional guidance; C.C., C.Z. and W.Z. revised this paper.

Funding: This research received funding from Project of State Grids Corporation of China (Project No. 5201011600TS).

Acknowledgments: This work was supported by the National Natural Science Foundation of China (Project No. 51477174), Project of State Grids Corporation of China (Project No. 5201011600TS), and the National Natural Science Foundation of China-UK Royal Society International Cooperation & Exchange Program (Project No. 517111530227).

Conflicts of Interest: The authors declare no conflict of interest.

References

1. Baccino, F.; Conte, F.; Grillo, S.; Massucco, S.; Silvestro, F. An optimal model-based control technique to improve wind farm participation to frequency regulation. *IEEE Trans. Sustain. Energy* **2015**, *6*, 993–1003. [CrossRef]
2. Makarov, Y.V.; Loutan, C.; Ma, J.; de Mello, P. Operational impacts of wind generation on California power systems. *IEEE Trans. Power Syst.* **2009**, *24*, 1039–1050. [CrossRef]
3. Liu, J.; Yao, Q.; Liu, Y.; Yang, H. Wind farm primary frequency control strategy based on wind & thermal power joint control. *Proc. CSEE* **2017**, *37*, 3462–3469.

4. Aho, J.; Buckspan, A.; Laks, J.; Fleming, P.; Jeong, Y.; Dunne, F.; Churchfield, M.; Pao, L.; Johnson, K. A tutorial of wind turbine control for supporting grid frequency through active power control. In Proceedings of the American Control Conference (ACC), Montreal, QC, Canada, 27–29 June 2012.
5. Morren, J.; de Haan, S.W.H.; Kling, W.L.; Ferreira, J.A. Wind turbines emulating inertia and supporting primary frequency control. *IEEE Trans. Power Syst.* **2006**, *21*, 433–434. [CrossRef]
6. Tang, X.; Miao, F.; Qi, Z.; He, H.; Wu, T.; Li, S. Survey on frequency control of wind power. *Proc. CSEE* **2014**, *34*, 4304–4314.
7. Wu, Z.; Gao, W.; Gao, T.; Yan, W.; Zhang, H.; Yan, S.; Wang, X. State-of-the-art review on frequency response of wind power plants in power systems. *J. Mod. Power Syst. Clean Energy* **2018**, *6*, 1–16. [CrossRef]
8. Li, L.; Ye, L. Coordinated control of frequency and rotational speed for direct drive permanent magnet synchronous generator wind turbine at variable wind speeds. *Autom. Electr. Power Syst.* **2011**, *35*, 26–31.
9. Wang, Y.; Delille, G.; Bayem, H.; Guillaud, X.; Francois, B. High wind power penetration in isolated power systems-assessment of wind inertial and primary frequency responses. *IEEE Trans. Power Syst.* **2013**, *28*, 2412–2420. [CrossRef]
10. Qian, D.; Tong, S.; Liu, H.; Liu, H. Load frequency control by neural-network-based integral sliding mode for nonlinear power systems with wind turbines. *Neurocomputing* **2016**, *173*, 875–885. [CrossRef]
11. Zhang, Z.; Sun, Y.; Li, G.; Cheng, L.; Lin, J. Frequency regulation by double fed induction generator wind turbines based on coordinated overspeed control and pitch control. *Autom. Electr. Power Syst.* **2011**, *35*, 20–25.
12. Wu, Z.; Gao, W.; Wang, J.; Gu, S. A coordinated primary frequency regulation from permanent magnet synchronous wind turbine generation. In Proceedings of the IEEE in Power Electronics and Machines in Wind Applications (PEMWA), Denver, CO, USA, 16–18 July 2012; IEEE: Piscataway, NJ, USA; pp. 1–6.
13. Liao, Y.; He, J.; Yao, J.; Zhang, K. Power smoothing control strategy of direct-driven permanent magnet synchronous generator for wind turbine with pitch angle control and torque dynamic control. *Proc. CSEE* **2009**, *29*, 71–77.
14. Chang-Chien, L.R.; Sun, C.C.; Yeh, Y.J. Modeling of wind farm participation in AGC. *IEEE Trans. Power Syst.* **2013**, *29*, 1204–1211. [CrossRef]
15. El Mokadem, M.; Courtecuisse, V.; Saudemont, C.; Robyns, B.; Deuse, J. Fuzzy logic supervisor-based primary frequency control experiments of a variable-speed wind generator. *IEEE Trans. Power Syst.* **2009**, *24*, 407–417. [CrossRef]
16. Zhao, J.; Lv, X.; Fu, Y.; Hu, X. Dynamic frequency control strategy of wind/photovoltaic/diesel microgrid based on DFIG virtual inertia control and pitch angle control. *Proc. CSEE* **2015**, *35*, 3815–3822.
17. Ye, X.; Lu, Z.; Qiao, Y.; Min, Y.; Huang, Q.; Wang, N. Hierarchical coordinated idea of wind and thermal power bundled transmission system. *Autom. Electr. Power Syst.* **2014**, *38*, 1–8.
18. Zhang, B.; Wu, W.; Zheng, T.; Sun, H. Design of a multi-time scale coordinated active power dispatching system for accommodating large scale wind power penetration. *Autom. Electr. Power Syst.* **2011**, *35*, 1–6.
19. Xi, Y. *Predictive Control*; National Defense Industry Press: Beijing, China, 2013.
20. Zheng, Y.; Zhou, J.; Xu, Y.; Zhang, Y.; Qian, Z. A distributed model predictive control based load frequency control scheme for multi-area interconnected power system using discrete-time Laguerre functions. *ISA Trans.* **2017**, *68*, 127–140. [CrossRef] [PubMed]
21. Ersdal, A.M.; Imsland, L.; Uhlen, K.; Fabozzi, D.; Thornhill, N.F. Model predictive load-frequency control taking into account imbalance uncertainty. *Control Eng. Pract.* **2016**, *53*, 139–150. [CrossRef]
22. Liu, X.; Zhang, Y.; Lee, K.Y. Robust distributed MPC for load frequency control of uncertain power systems. *Control Eng. Pract.* **2016**, *56*, 136–147. [CrossRef]
23. Zhao, H.; Wu, Q.; Wang, J.; Liu, Z.; Shahidehpour, M.; Xue, Y. Combined active and reactive power control of wind farms based on model predictive control. *IEEE Trans. Energy Convers.* **2017**, *32*, 1177–1187. [CrossRef]
24. Ye, L.; Ren, C.; Li, Z.; Yao, Y.; Zhao, Y. Stratified progressive predictive control strategy for multi-objective dispatching active power in wind farm. *Proc. CSEE* **2016**, *36*, 6327–6336.
25. Makarov, Y.V.; Etingov, P.V.; Ma, J.; Huang, Z.; Subbarao, K. Incorporating uncertainty of wind power generation forecast into power system operation, dispatch, and unit commitment procedures. *IEEE Trans. Sustain. Energy* **2011**, *2*, 433–442. [CrossRef]
26. Zhang, B.; Chen, J.; Wu, W. A hierarchical model predictive control method of active power for accommodating large-scale wind power integration. *Autom. Electr. Power Syst.* **2014**, *38*, 6–14.

27. Kaddah, S.S.; Abo-Al-Ez, K.M.; Megahed, T.F. Application of nonlinear model predictive control based on swarm optimization in power systems optimal operation with wind resources. *Electr. Power Syst. Res.* **2017**, *143*, 415–430. [CrossRef]
28. Xie, L.; Ilic, M.D. Model predictive economic/environmental dispatch of power systems with intermittent resources. In Proceedings of the 2009 IEEE Power & Energy Society General Meeting (PES'09), Calgary, AB, Canada, 26–30 July 2009; IEEE: Piscataway, NJ, USA; pp. 1–6.
29. Xie, L.; Ilic, M.D. Model predictive dispatch in electric energy systems with intermittent resources. In Proceedings of the 2008 IEEE International Conference on Systems, Man and Cybernetics (SMC 2008), Singapore, 12–15 October 2008; IEEE: Piscataway, NJ, USA; pp. 42–47.
30. Variani, M.H.; Tomsovic, K. Distributed automatic generation control using flatness-based approach for high penetration of wind generation. *IEEE Trans. Power Syst.* **2013**, *28*, 3002–3009. [CrossRef]
31. Mohamed, T.H.; Morel, J.; Bevrani, H.; Hiyama, T. Model predictive based load frequency control_design concerning wind turbines. *Int. J. Electr. Power Energy Syst.* **2012**, *43*, 859–867. [CrossRef]
32. Mohamed, T.H.; Bevrani, H.; Hassan, A.A.; Hiyama, T. Decentralized model predictive based load frequency control in an interconnected power system. *Energy Convers. Manag.* **2011**, *52*, 1208–1214. [CrossRef]
33. Zheng, Y.; Li, S.; Qiu, H. Networked coordination-based distributed model predictive control for large-scale system. *IEEE Trans. Control Syst. Technol.* **2013**, *21*, 991–998. [CrossRef]
34. Zhang, Y.; Liu, X.; Qu, B. Distributed model predictive load frequency control of multi-area power system with DFIGs. *IEEE/CAA J. Autom. Sin.* **2017**, *4*, 125–135. [CrossRef]
35. Venkat, A.N.; Hiskens, I.A.; Rawlings, J.B.; Wright, S.J. Distributed MPC strategies with application to power system automatic generation control. *IEEE Trans. Control Syst. Technol.* **2008**, *16*, 1192–1206. [CrossRef]
36. Bevrani, H.; Daneshfar, F.; Hiyama, T. A new intelligent agent-based AGC design with real-time application. *IEEE Trans. Syst. Man Cybern. Part C (Appl. Rev.)* **2012**, *42*, 994–1002. [CrossRef]
37. Ma, M.; Liu, X.; Zhang, C. LFC for multi-area interconnected power system concerning wind turbines based on DMPC. *IET Gener. Transm. Distrib.* **2017**, *11*, 2689–2696. [CrossRef]
38. Ma, M.; Zhang, C.; Shao, L.; Sun, Y. Primary frequency regulation for multi-area interconnected power system with wind turbines based on DMPC. In Proceedings of the 2016 35th Chinese Control Conference, Chengdu, China, 27–29 July 2016; IEEE: Piscataway, NJ, USA, 2016; pp. 4384–4389.
39. Casavola, F.T.A. Fault-tolerant distributed load/frequency supervisory strategies for networked multi-area microgrids. *Int. J. Robust Nonlinear Control* **2014**, *24*, 1380–1402.
40. Fu, Y.; Wang, Y.; Zhang, X.; Luo, Y. Analysis and integrated control of inertia and primary frequency regulation for variable speed wind turbines. *Proc. CSEE* **2014**, *34*, 4706–4716.
41. Chien, L.R.C.; Lin, W.T.; Yin, Y.C. Enhancing frequency response control by DFIGs in the high wind penetrated power systems. *IEEE Trans. Power Syst.* **2011**, *26*, 710–718. [CrossRef]
42. Almeida, R.G.; Lopes, J.A.P. Participation of doubly fed induction wind generators in system frequency regulation. *IEEE Trans. Power Syst.* **2007**, *22*, 944–950. [CrossRef]
43. Leea, H.J.; Jin, B.P.; Jooc, Y.H. Robust load-frequency control for uncertain nonlinear power systems: A fuzzy logic approach. *Inf. Sci.* **2006**, *176*, 3520–3537. [CrossRef]
44. Bevrani, H. *Robust Power System Frequency Control*; Springer: New York, NY, USA, 2009.
45. Ye, L.; Zhu, Q.; Zhao, Y. Dynamic optimal combination model considering adaptive exponential for ultra-short term power prediction. *Autom. Electr. Power Syst.* **2015**, *39*, 12–18.